INSTITUT DE FRANCE
Académie des sciences

Comptes Rendus

Géoscience

Sciences de la Planète

Nicolas Tribovillard, Viviane Bout-Roumazeilles, François Guillot, François Baudin, Jean-François Deconinck, Romain Abraham and Sandra Ventalon

A sedimentological oxymoron: highly evolved glauconite of earliest diagenetic origin

Volume 355 (2023), p. 157-173

Published online: 28 April 2023

https://doi.org/10.5802/crgeos.208

Les Comptes Rendus. Géoscience — Sciences de la Planète *sont membres du Centre Mersenne pour l'édition scientifique ouverte*
www.centre-mersenne.org
e-ISSN : 1778-7025

Comptes Rendus
Géoscience — Sciences de la Planète
2023, Vol. 355, p. 157-173
https://doi.org/10.5802/crgeos.208

Original Article — Petrology, Sedimentology

A sedimentological oxymoron: highly evolved glauconite of earliest diagenetic origin

Nicolas Tribovillard [a, *], Viviane Bout-Roumazeilles [a], François Guillot [a], François Baudin [b], Jean-François Deconinck [c], Romain Abraham [a] and Sandra Ventalon [a]

[a] Université de Lille, UMR 8187 LOG – Laboratoire d'Océanologie et de Géosciences, Univ. Lille, CNRS, Univ. Littoral Côte d'Opale, IRD, 59000 Lille, France

[b] Sorbonne Université - CNRS, UMR 7193 ISTeP - Institut des Sciences de la Terre de Paris, 75005 Paris, France

[c] Université de Bourgogne - CNRS, UMR 6282 Biogéosciences, 21000 Dijon, France

E-mails: nicolas.tribovillard@univ-lille.fr (N. Tribovillard), viviane.roumazeilles@univ-lille.fr (V. Bout-Roumazeilles), francois.guillot@univ-lille.fr (F. Guillot), francois.baudin@sorbonne-universite.fr (F. Baudin), jean-francois.deconinck@u-bourgogne.fr (J.-F. Deconinck), romain.abraham@univ-lille.fr (R. Abraham), sandra.ventalon@univ-lille.fr (S. Ventalon)

Abstract. This work examines the possibility of a rapid formation of glauconite in a relatively shallow platform environment (below fair-weather wave baseline). The materials studied here are uppermost Jurassic alternations of carbonate beds and marly interbeds, namely, the Assises de Croï Formation of the Boulonnais area (northernmost France). The carbonate beds yield field evidences of an early diagenetic origin and both beds and interbeds contain glauconite, questioning the duration of formation of the glauconite, relative to that of the diagenetic carbonate beds. Carbon and oxygen stable isotope composition of the carbonate beds confirm an early diagenetic growth. Contrasted grain-size distribution patterns of glauconite and quartz grain populations (isolated after acid digestion and magnetic separation) evidenced that glauconite formed after sediment deposition. Glauconite formation allegedly requires protracted episodes of ion capture from the water column, which is no longer possible when glauconite gets trapped within authigenic carbonates. Therefore, *in-situ* glauconite formation preceded carbonate authigenesis. Yet, the chemical composition of grains (Fe and K) typifies glauconite as highly evolved, meaning that its formation must have lasted over times, according to conventional views. Consequently, our results challenge these conventional views and confirm that glauconite can form in relatively shallow environments (which has been already brought to light previously) and it is concluded that early diagenetic glauconite can be markedly enriched in both K and Fe, which is an unprecedented result.

Keywords. Glauconite, Late Jurassic, Tithonian, Boulonnais, Authigenic minerals, Diagenesis.

Manuscript received 13 January 2023, revised 23 March 2023, accepted 30 March 2023.

* Corresponding author.

1. Introduction

Glauconite is a fairly common authigenic mineral belonging to the family of green clay minerals often grouped under the term glaucony [Odin and Matter, 1981, Velde, 2014, Huggett, 2021, to mention a few]. Glauconite is a potassium- and iron-rich phyllosilicate. It is commonly accepted that glauconite is a marine mineral the growth of which is slow, therefore requiring protracted exchanges with sea water, so that seawater ions can be incorporated into the crystal lattices of these neoformed phyllosilicates. Therefore, glauconite is generally considered to grow in environments where the sedimentation rate is low and iron and potassium are relatively abundant in the water column. The "ideal" location for the authigenic formation of this mineral is therefore often considered to be the distal edge of the continental shelf. Alongside this common view, numerous studies have reported that glauconite could also appear in shallow environments, such as estuaries or deltas, or even river environments [e.g., El Albani et al., 2005, Meunier and El Albani, 2007, and references therein; Wilmsen and Bansal, 2021, Bansal et al., 2022]. Therefore, the speed of formation of glauconite can also be questioned: if the formation of this mineral is possible in proximal environments, where sedimentation rates can be high, then the contact time between authigenic minerals and seawater column cannot be extremely long [Wilmsen and Bansal, 2021]. To try and clarify the question of the rapidity of the formation of glauconite, we chose to study Jurassic age deposits from Boulonnais (N-France) cropping out along the cliffs of the Pas de Calais (Strait of Dover) between England and France (English Channel; Figure 1). These deposits constitute the geological formation of the Assises de Croï; they form a limestone–marl alternation, visually rich in glauconite, where the limestone beds show evidences of a diagenetic origin (Figures 2 and 3). If these limestone beds are indeed diagenetic, then the questions are: (1) whether it is early or late diagenesis, (2) whether the glauconite they contain is itself authigenic and autochthonous and (3) whether this glauconite was formed before or after the limestone beds. Depending on the answers to these questions, a very early formation of glauconite can be inferred. The Assises de Croï Fm. is therefore an object of study of primary importance relative to the above questions. This work is based on (1) field observations and sampling, (2) the determination of the stable isotope signature (C, O) of the carbonate beds, making it possible to evaluate the origin of the carbonates, (3) Rock Eval analysis providing sedimentary parameters, (4) the separation of glauconite and quartz grains from beds and interbeds in order to observe their morphology, determine their grain size patterns and perform *in-situ* chemical analyses using a scanning electron microscope. Finally, even if this is not its primary goal, this study is part of a stratigraphic project aimed at better defining the Jurassic-Cretaceous boundary in the Boulonnais, currently led by J.-F. Deconinck.

2. Geological background

The Assises de Croï Formation (Fm.), formerly called Marnes et Calcaires à *Ostrea expansa* [Bonte, 1969] and also called Argiles et Calcaires de la Tour de Croï [Mansy et al., 2007], is dated of the Upper Tithonian and includes ammonites from the Albani, Glaucolithus and *pro parte* Okusensis ammonite zones [Townson and Wimbledon, 1979, Geyssant et al., 1993, Herbin et al., 1995, Deconinck et al., 1996, Deconinck and Baudin, 2008]. Good outcrops exist south and north of Wimereux (spots 1 and 2, respectively), notably south of Pointe aux Oies (Figure 1). About ten meters thick, this formation is characterized by an alternation of nodular and glauconitic limestone beds, from one part, and silty and glauconitic marls from the other part. The bounding surfaces between carbonate beds and marly interbeds are fairly contorted (Figures 2 and 3). The carbonate beds, more or less discontinuous, made of loosely jointed, cauliflower-sized patches show numerous bioturbations and seem to have been formed by the induration of a dense network of burrows of the *Thalassinoides* type. This induration must have been precocious, occasionally allowing the installation of a fauna of oysters and, sometimes, boring organisms. The limit between the underlying Argiles de Wimereux Fm. and the Assises de Croï is visible at the foot of the cliff south of Wimereux (spot 1) and south of Pointe aux Oies (spot 2): the first carbonate beds mark a morphological break between the beach and the cliff (Figures 2 and 3). The Assises de Croï is covered by the Grès des Oies corresponding to the Okusensis zone (*pro parte*) and to the Kerberus zone

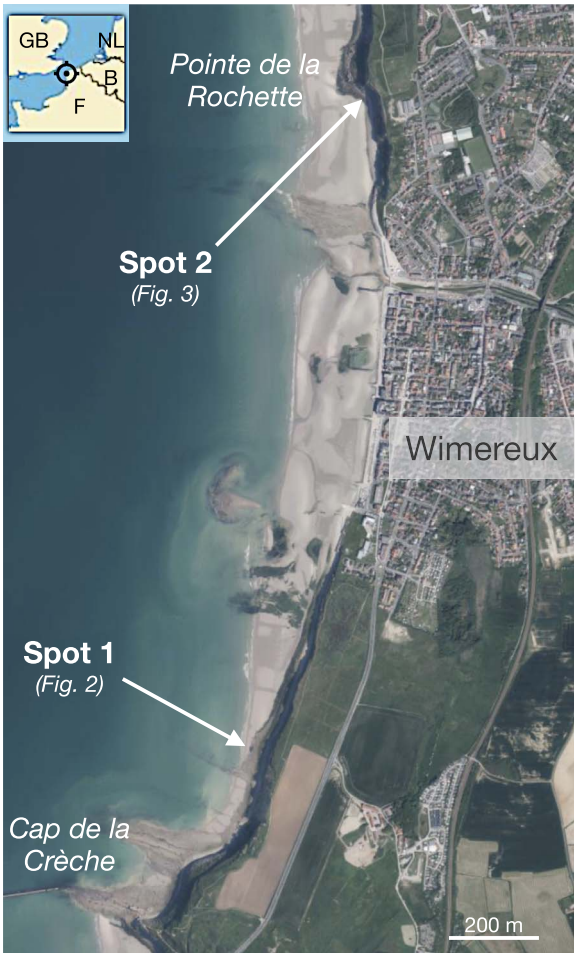

Spot 1: latitude 50.775210°, longitude 1.605825°
Spot 2: latitude 50.755394°, longitude 1.600550°

Figure 1. Location of the two outcrops examined south and north of Wimereux, on the so-called Côte d'Opale or Opal Coast. The outcrops are illustrated with Figures 2 and 3. Source: Institut Géographique National.

[Deconinck and Baudin, 2008]. These are fine sandstones with carbonated cement containing many bivalves (*Cardium* and *Trigonia* in particular).

Townson and Wimbledon [1979] divided the formation into three parts, based on sedimentological observations. Their interpretations may be summarized as follows: the Lower Assises de Croï was deposited relatively rapidly with little time for biological homogenization of silt-clay-lime mud cycles. The sedimentation rate must have slowed down during deposition of the Middle Assises de Croï, as evidenced by the high concentration of glauconite, presence of phosphate, intense bioturbation and locally present encrusted or bored surfaces. The presence of coarse quartz sand and chert granules suggests that the areas of land-derived supply were close but glauconite and *Rhizocorallium* suggest low energy middle neritic conditions. Shallowing kept on during deposition of the Upper Assises de Croï, as indicated by the presence of large *Thalassinoides* and the lower glauconite content, but the coarse clastic supply decreased. Deposition of lime mud was common and a diversified echinoid and bivalve fauna flourished in medium to low-energy, inner to middle neritic, conditions [Townson and Wimbledon, 1979]. Noteworthy, the interpretations of these authors imply that the glauconite was authigenic and syn-deposit, which we intend to test here.

3. Materials and methods

Only the Lower and Middle Assises de Croï were examined, because the cliff-forming upper part of the formation was not easy to sample with current outcrop conditions (Figures 2 and 3). Eight carbonate beds and seven marly interbeds were sampled at spot 2, north off Wimereux (Table 1).

Usual Rock-Eval analysis parameters [Baudin, 2023] have been measured at the ISTeP lab of Sorbonne University (Paris) on bulk-rock samples using the latest Rock-Eval apparatus (RE-7S, Vinci Technologies), which is an evolution of the RE-6 model [Behar et al., 2001] allowing the sulfur products to be monitored during gradual heating in sequential and combustion cycles [Lamoureux-Var et al., 2019, Cohen-Sadon et al., 2022, Baudin, 2023].

The carbon and oxygen isotope composition have been determined at the Biogeosciences lab of University of Dijon from the samples of carbonate beds, using a Kiel IV preparation device coupled with a Thermofisher Delta V Plus mass spectrometer. Powdered carbonate samples were digested using 20 µl of orthophosphoric acid at 70 °C. The reproducibility (2σ) of the IAEA NBS19, used as an external standard, is better than 0.04‰ for the δ^{13}C and 0.08‰ for the δ^{18}O. The δ notation is expressed relatively to the V-PDB (Vienna Pee Dee Belemnite).

At the LOG lab of University of Lille, the glauconite grains were isolated through the protocol described in Tribovillard et al. [2021, 2023]. Briefly, samples

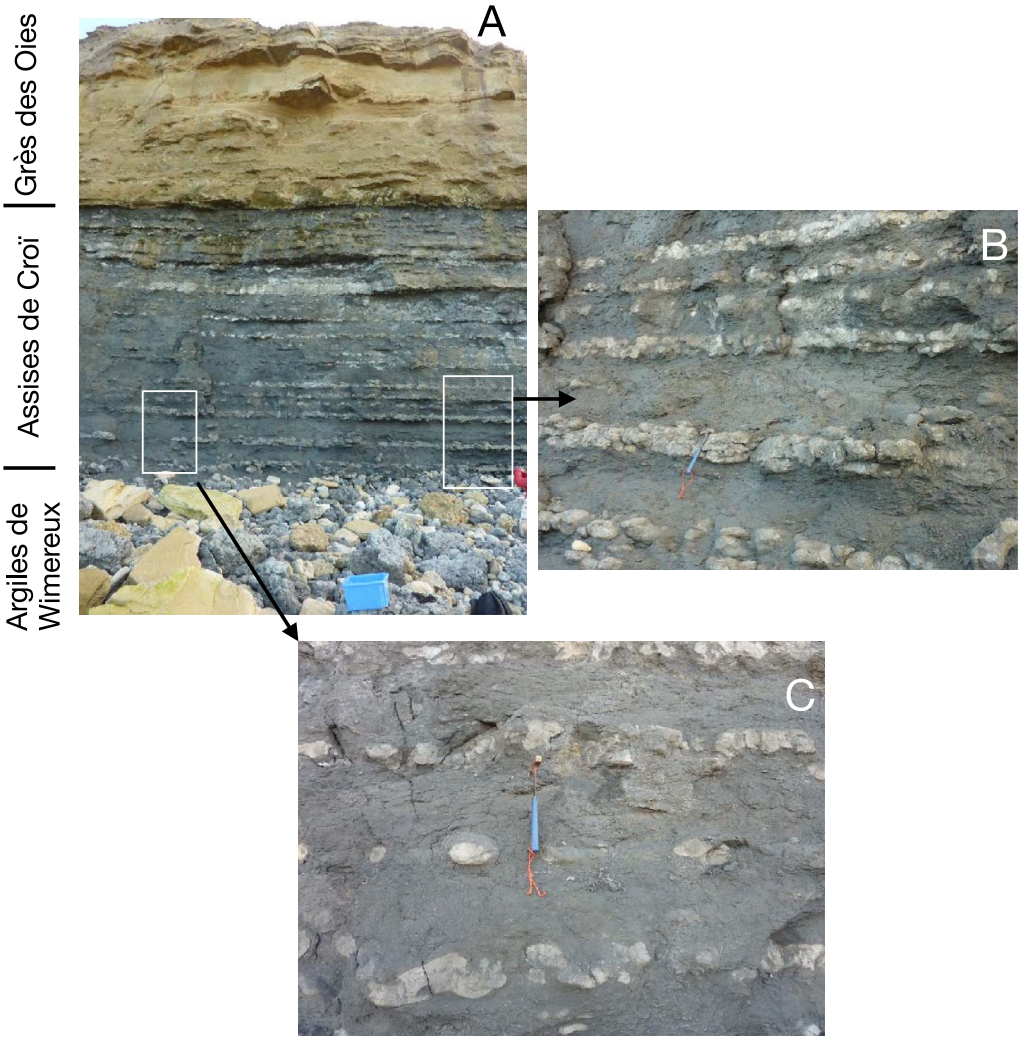

Figure 2. Spot 1, south of Wimereux, where the topmost deposits of the Jurassic are visible. Yellowish top beds of the cliff belong to the Grès des Oies Fm.

were digested with HCl to dissolve the carbonate and phosphate phases before being rinsed. Several rinses were carried out after the necessary time for grains coarser than clays to settle and for clays to be removed with the supernatant. This operation was repeated at least 20 times, until the liquid kept limpid. What remained in the beakers was grains of glauconite and quartz (plus some accessory minerals). Glauconite was then separated from quartz using a Frantz magnetic separator. The grain size of the glauconite and quartz particles was studied using a laser beam-equipped analyzer Malvern MasterSizer [protocol in Trentesaux et al., 2001]. Two indices have been calculated: sorting and skewness *sensu* Trask. Sorting (So) is defined as the square root of the ratio of the 75th and 25th percentiles (Q75 and Q25): $So = \sqrt{(Q75 \div Q25)}$; skewness (Sk) is defined as the product of Q75 and Q25 divided by the square of the median: $Sk = (Q25 \times Q75) \div Md^2$.

The glauconite particles were imaged using a scanning electron microscope (SEM) equipped with a EDS-type analytical probe. The grains were also analyzed by X-ray diffraction (XRD) to determine their mineralogy according to the standard protocol described in Bout-Roumazeilles et al. [1999]. XRD was performed both on oriented mounts and

Figure 3. Spot 2, north of Wimereux. The cliff-forming part of the Assises de Croï Fm. (A) with, at its base, alternations of marly levels (B) and carbonate nodular beds (C,D).

non-oriented ones to fully discriminate glauconite from illite.

4. Results

4.1. *Rock-Eval analysis*

The parameters of the Rock-Eval analysis show that (1) total organic carbon (TOC) values keep low (<0.8 wt%) and (2) all the samples yield low values for both the T_{max} and Hydrogen Index (HI) (Table 1). It must be kept in mind that when TOC values are low, Hi, OI and T_{max} parameters must be considered with caution, which is the case here for most of the samples [Baudin, 2023]. However, in a T_{max} versus HI diagram [Espitalié et al., 1986, Figure 4], all the values are rather close, pointing to a Type III organic matter (OM), that is, a highly degraded OM of probable

Table 1. Rock Eval parameters of the samples studied

Samples	T_{max} (°C)	HI *(1)*	OI *(2)*	TOC (%)	MINC (%)	$CaCO_3$ (%)	Total S (%)	Weight % glauconite in the HCl-insoluble fraction	CFB TOC (%)	CFB S (%)
Carbonate bed A1	391	47	367	0.18	5.43	45.25	0.54	7	0.3	1.0
Carbonate bed A2	397	123	457	0.2	10.23	85.25	0.27	6	1.4	1.8
Interbed A	425	54	84	0.79	1.58	13.17	1.59	11	0.9	1.8
Carbonate bed B	416	53	388	0.12	9.04	75.33	0.26	16	0.5	1.1
Interbed B	421	37	117	0.55	2.01	16.75	1.01	20	0.7	1.2
Carbonate bed C	422	61	283	0.18	8.31	69.25	0.31	15	0.6	1.0
Interbed C	422	51	145	0.5	1.84	15.33	0.82	17	0.6	1.0
Carbonate bed D	378	74	438	0.17	9.3	77.50	0.36	8	0.8	1.6
Interbed D	422	61	136	0.44	2.77	23.08	0.96	13	0.6	1.2
Carbonate bed E	354	44	678	0.16	6.95	57.92	0.27	14	0.4	0.6
Interbed E	414	24	169	0.27	0.99	8.25	1.24	21	0.3	1.4
Carbonate bed F	411	62	502	0.06	10.39	86.58	0.16	6	0.4	1.2
Interbed F	407	42	196	0.32	2.33	19.42	0.69	7	0.4	0.9
Carbonate bed G	429	56	253	0.17	10.14	84.50	0.36	5	1.1	2.3
Interbed G	426	84	104	0.45	4.17	34.75	0.92	6	0.7	1.4
Carbonate beds, mean values	**400**	***65***	***421***	**0.16**	**8.7**	**72.7**	**0.32**	**10**	0.6	1.2
Marly Interbeds, mean values	**420**	**50**	**136**	**0.47**	**2.2**	**18.7**	**1.03**	**14**	0.6	1.3

TOC stands for total organic carbon (expressed in weight %). HI stands for hydrogen index and is expressed in g hydrocarbons per g of TOC; OI or oxygen index, is in mg CO_2 per g TOC [Espitalié et al., 1986]. The Rock-Eval 7 apparatus yields the sulfur abundance and speciation, as well as the concentration in inorganic C (MinC), allowing the $CaCO_3$ content to be calculated. CFB stands for carbonate-free basis.

terrestrial, possibly marine, origin, below the lower boundary of the oil-window stage of organic maturation. In addition to the usual parameters regarding OM, the Rock-Eval 7 apparatus measures the inorganic C content (called MinC in the Rock-Eval terminology) as well as the various forms of sulfur (sulfate, sulfide, organic S). In the present case, sulfur is only present in the form of pyrite. On average, S content is higher in the marly interbeds than in the carbonate beds (Table 1). The same is true for the TOC values. However, the MinC parameter allows the theoretical $CaCO_3$ content to be derived ($[CaCO_3] = MinC \times 100 \div 12$; Table 1). Thus the TOC and S contents can be calculated on a carbonate-free basis (CFB).

$$TOC_{CFB} = TOC \times 100 \div (100 - [CaCO_3])$$

and

$$S_{CFB} = [S] \times 100 \div (100 - [CaCO_3]).$$

On such a carbonate-free basis, the averaged differences between carbonate beds and marly interbeds are erased for both TOC and S contents (Table 1). Keeping with the HCl-insoluble fractions of the sediments, the weight proportion of glauconite compared to the carbonate-free part of the samples studied is higher for the interbeds than for the beds (Table 1).

4.2. *C and O isotope composition*

Among the eight carbonate beds sampled, seven show $\delta^{13}C$ and $\delta^{18}O$ values that are quite close, while one sample (bed A1) shows a somewhat higher value for $\delta_{13}C$ and a lower one for $\delta_{18}O$ (Figure 5, with zero value for normal seawater, and Table 2). The value of the group of 8 samples are bracketed within the following range: [−1.159‰ : 0.9‰] for $\delta^{13}C$ (mean: −0.279‰) and [−2.47‰ : −1.318‰] for $\delta_{18}O$ (mean: −1.728‰).

4.3. *Mineralogy and grain size distribution*

In agreement with our previous work conducted in the Upper Jurassic rocks and Cretaceous chalk of

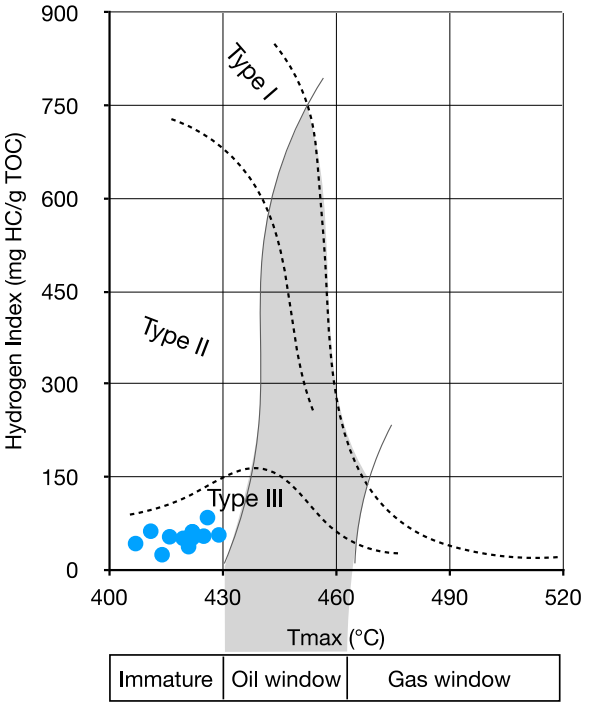

Figure 4. HI–T_{max} diagram [Espitalié et al., 1986], based on Rock-Eval analysis data, shows that the organic matter of the samples examined here is of Type III [all details about Rock-Eval in Baudin, 2023].

Table 2. Stable isotope composition of C and O for the eight carbonate beds sampled

Sample	δ^{13}C (‰)	δ^{18}O (‰)
Bed A1	0.93	−2.47
Bed A2	−0.516	−1.318
Bed B	0.16	−1.372
Bed C	−0.84	−1.886
Bed D	−0.318	−1.802
Bed E	−0.828	−1.747
Bed F	−1.159	−1.615
Bed G	0.339	−1.615

the Boulonnais area [Tribovillard et al., 2021, 2023], the green minerals in the samples studied here were identified as glauconite using XRD (Supplementary Figure S1). The glauconite shows a high crystallinity

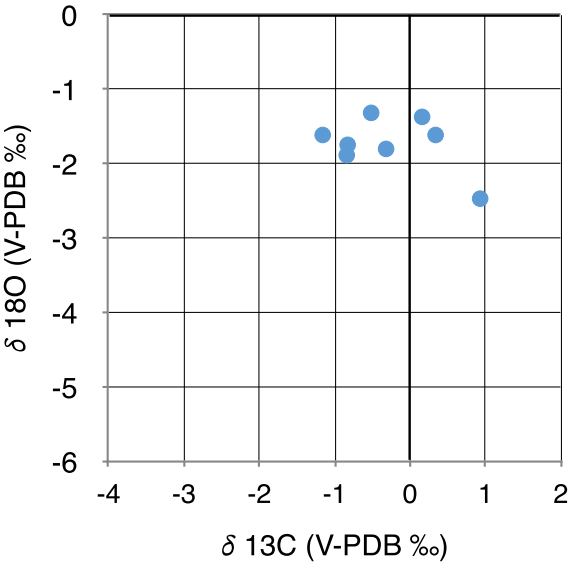

Figure 5. Diagram combining stable isotope compositions for O and C, measured on the carbonate beds sampled at spot 2.

index [0.4° 2 theta; Deconinck et al., 1982]. The HCl-leached fraction of the rock samples contains quasi-exclusively quartz and glauconite. These two mineral species were efficiently separated using a magnetic separator and could be analyzed separately. The grain size analyzes are presented in Table 3 and illustrated with Figures 6 and 7. The populations of quartz grains show a unimodal size distribution, whereas the glauconite populations show bimodal grain size distribution. Figure 6 gathers the typical curves of grain size distribution for quartz and glauconite, whether they come from carbonate beds or from marly interbeds.

Again, as in the previous works cited above, the grain size distribution shows the presence of very small particles of the order of a micrometer or less, drawing a sort of bump in the curves (Figure 6). These particles, once sampled and analyzed using XRD, turned out to be glauconite as well. The glauconite grain extraction protocol should normally lead to the elimination of particles of this size; their presence is explained by mechanical wear of the grains during the particle size analysis, generated by the current of fluid circulating in front of the laser beam. This flow of water generates shocks capable of tearing tiny particles from larger grains.

Table 3. Selected grain-size parameters for the two populations of grains (glauconite and quartz) extracted from beds and interbeds

Samples	Median (μm)	Mean (μm)	Mode (μm)	So	Sk
Bed A1 glauconite	9.95	14.08	21.15	7.77	
Bed A2 glauconite	7.29	11.70	18.18	7.98	
Bed B glauconite	8.64	12.13	17.26	6.55	
Bed C glauconite	14.24	18.29	25.09	3.23	
Bed D glauconite	12.74	16.16	21.73	3.08	
Bed E glauconite	66.52	71.31	82.32	1.65	
Bed F glauconite	9.72	13.35	18.84	6.24	
Bed G glauconite	10.97	15.20	20.26	3.06	
Mean value	***17.51***	***21.53***	***28.10***	***4.95***	
Bed A1 quartz	169.11	184.60	180.17	1.43	0.97
Bed A2 quartz	184.42	198.07	190.42	1.36	0.99
Bed B quartz	150.03	164.10	165.94	1.51	0.95
Bed C quartz	162.86	175.48	178.59	1.45	0.96
Bed D quartz	134.18	145.04	148.42	1.48	0.95
Bed E quartz	148.30	159.79	149.25	1.34	1.00
Bed F quartz	137.96	149.08	147.30	1.44	0.97
Bed G quartz	137.10	145.91	145.14	1.39	0.97
Mean value	***152.99***	***165.26***	***163.15***	***1.43***	***0.97***
Interbed A glauconite	18.59	23.90	34.60	3.02	
Interbed B glauconite	23.65	27.67	37.20	2.36	
Interbed C glauconite	84.99	91.93	99.55	1.56	
Interbed D glauconite	50.05	54.18	63.03	1.67	
Interbed E glauconite	41.14	46.12	54.79	1.81	
Interbed F glauconite	75.64	82.05	93.93	1.69	
Interbed G glauconite	32.74	39.45	47.58	2.00	
Mean value	***46.68***	***52.19***	***61.53***	***2.02***	
Interbed A quartz	162.44	174.20	177.19	1.45	0.96
Interbed B quartz	156.75	167.57	174.66	1.46	0.94
Interbed C quartz	173.03	185.43	183.48	1.40	0.97
Interbed D quartz	177.81	188.92	183.39	1.34	0.99
Interbed E quartz	139.17	146.22	160.27	1.51	0.91
Interbed F quartz	130.71	140.54	152.51	1.57	0.89
Interbed G quartz	130.77	135.14	152.21	1.52	0.89
Mean value	***152.95***	***162.57***	***169.10***	***1.46***	***0.96***

The sorting index (So) can be calculated for each sample but the skewness index (Sk) cannot be calculated for the multi modal distributions of the glauconite grains. The quartz grains are better sorted than the glauconite grains.

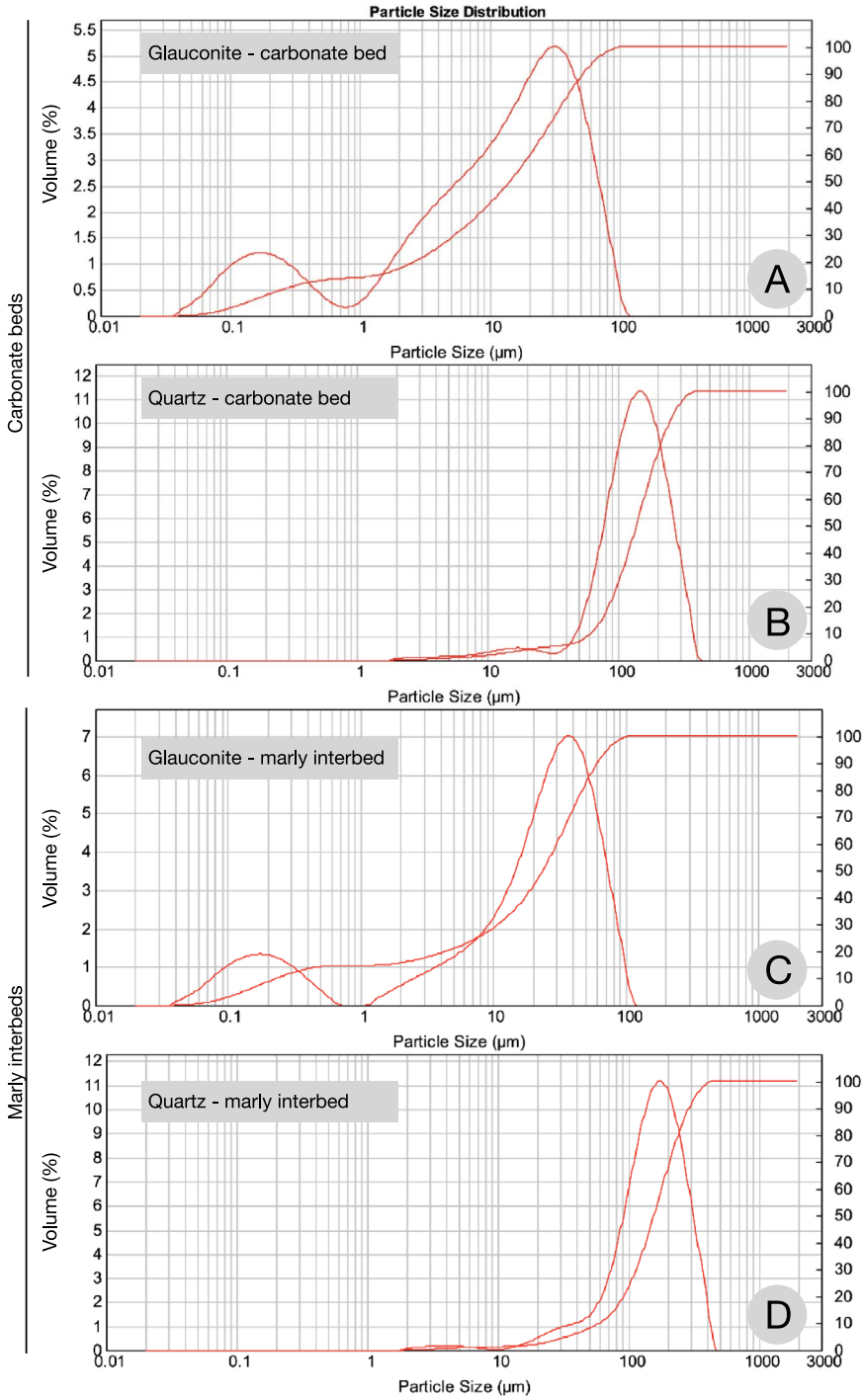

Figure 6. Illustration of the typical grain-size distribution of the glauconite and quartz grains of the carbonate beds and marly interbeds. Panels A and C show the characteristic bump (1 µm and less) observed with non-reworked glauconite grains (see text for explanations).

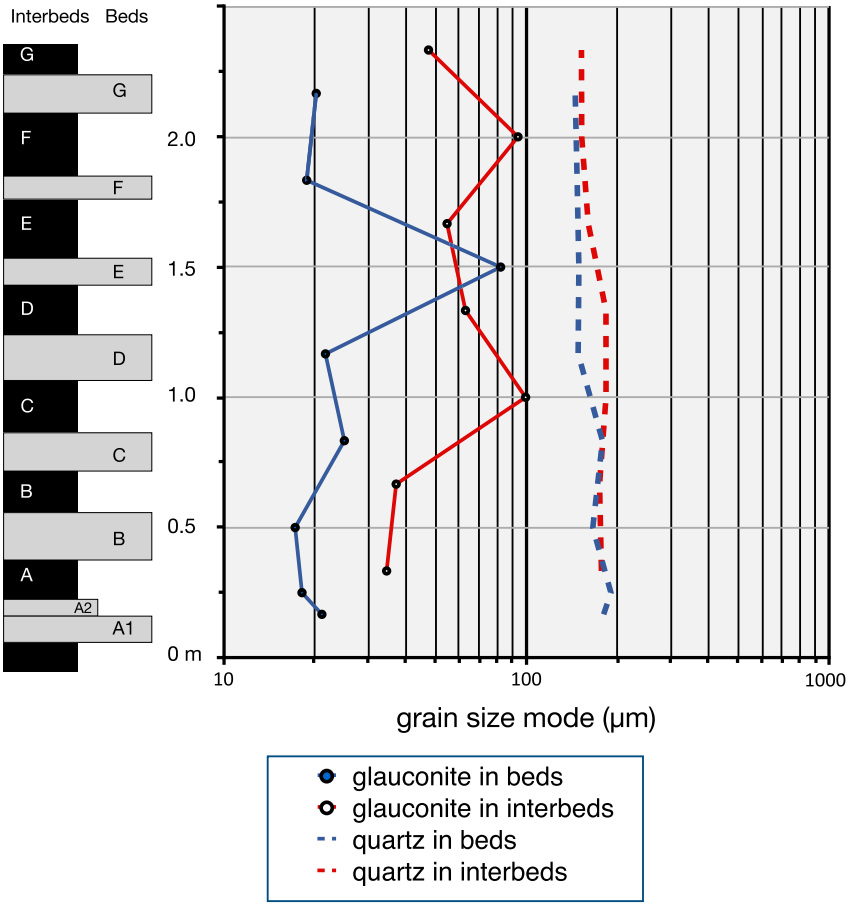

Figure 7. Vertical distribution of the mode value for quartz and glauconite in carbonate beds and marly interbeds. The modes of the quartz grain populations are almost constant, either in beds or in interbeds, whereas the glauconite grain populations show variable modes as well as differences between beds and interbeds.

4.4. *SEM imaging and chemical analyses*

SEM observation yields the aspect of the glauconite grains of the studied samples: the grains are rather homogeneous and strikingly different from those contained in sediments where glauconite is allochthonous (reworked) (Figure 8A). Reworked glauconite shows impact scars and streaks engraved on the surface of the grains (Figure 8B) that are not observed in the samples of the Assises de Croï Fm. Semi-quantitative analyses have been performed on individual grains using the EDS probe of the SEM. The concentrations in FeO and K_2O thus obtained are consistent with those obtained previously through OES techniques [Tribovillard et al., 2023]. As illustrated with Figure 8C, a correlation is drawn between the FeO and K_2O concentrations, and the concentrations of most of the samples are above the threshold values (K_2O > 8%, FeO > 22% or Fe_2O_3 > 24%) of the so-called highly evolved glauconite, first determined by Odin and Matter [1981]. The highly evolved feature is also evidenced by the excellent crystallinity mentioned above.

Lastly, no euhedral quartz minerals were observed using SEM or binocular stereo-microscopes, allowing the presence of syn-sediment-grown, authigenic quartz to be ruled out.

5. Discussion

Glauconite is found here both in carbonate beds and marly interbeds, together with quartz. Quartz

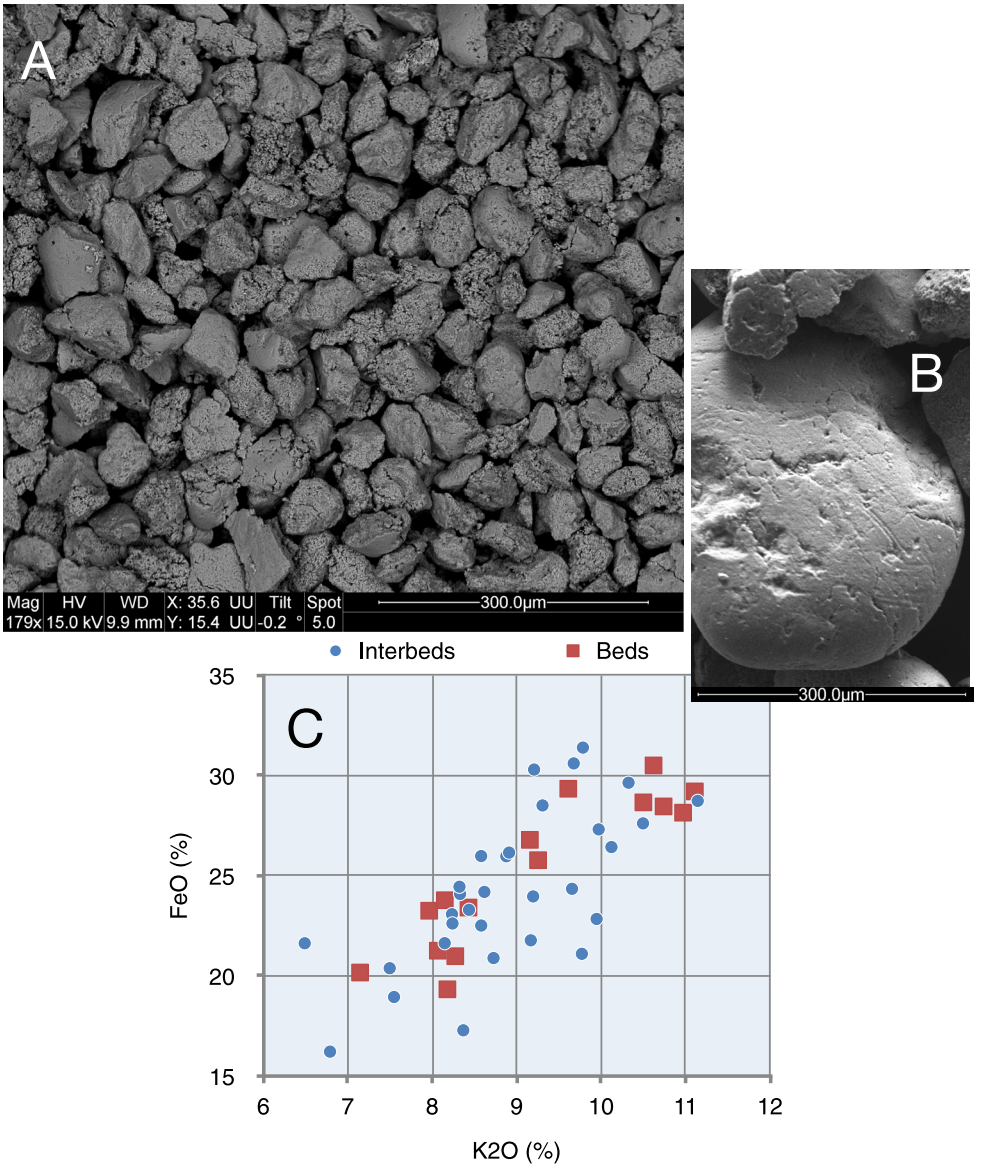

Figure 8. SEM imaging of the typical aspect of the glauconite grains of the Assises de Croï (A), to be compared with worn grains (B) of deposits containing reworked glauconite. Panel C shows the distribution of bed samples (red squares) and interbed samples (blue dots) when K and Fe concentrations are compared.

is not authigenic here but glauconite can be authigenic and syn-deposit (autochthonous) or reworked (allochthonous). Being able to distinguish the possible two origins is of cornerstone importance for the present work: if glauconite has grown authigenically within the sediment where it is still observed, it may be used as a proxy of depositional conditions. However, if glauconite has been reworked and has not grown *in situ*, it cannot be used to reconstruct the depositional conditions of the sediments where it is observed today.

5.1. *Syn-deposit glauconite*

This authigenic mineral is classically considered to form at the sediment–water interface (or in its

immediate vicinity) through protracted exchanges over time with seawater [Odin and Matter, 1981, Amorosi, 1995, Banerjee et al., 2012, 2016a,b, López-Quirós et al., 2020]. As some conditions required for the formation of glauconite at, or close to, the sediment–water interface, one can mention slow sedimentation rates permitting long-lasting availability of dissolved cations, together with oxygen-limited, mildly reducing, conditions [Odin and Matter, 1981, Meunier and El Albani, 2007, Roy Choudhury et al., 2021, Huggett, 2021]. Glauconite commonly appears as lobate grains (pellets), with frequent cracked surfaces [Boyer et al., 1977, Bayliss and Syvitski, 1982]. Along with its K_2O concentration, the morphologic characteristics of glauconite are used as criteria to estimate the duration of the authigenic formation of this mineral [Velde, 2014, and references therein]. Moreover, this mineral, which is physically resistant, is likely to be reworked and re-sedimented later, like quartz grains. Therefore, the presence of glauconite in a deposit does not automatically mean a local authigenic (and therefore syn-depositional) formation of this mineral. Recent work [Tribovillard et al., 2021, 2023] has shown that examining the grain size distribution curves of glauconite makes it possible to distinguish between syn-depositional glauconite and reworked glauconite.

5.1.1. *Carbonate beds*

Here, the grain size distribution of the HCl-insoluble particles of the carbonate beds shows that the quartz is well sorted, while the glauconite is not (Table 3). The difference between a well-sorted glauconite and an ill-sorted one can be illustrated with Figure 9 showing the grain size distribution curve of Cretaceous samples of Aptian–Albian glauconitic sand sampled in the Boulonnais (at the base of the Cap Blanc-Nez chalk massif). This well-sorted glauconite shows a size distribution curve similar to that of the companion quartz. In addition, the mode of the quartz grain curve is most often comprised between 100 μm and 200 μm, whereas the mode of the glauconite grain curve is between 10 μm and 30 μm (except for one sample), most often close to 20 μm. Therefore, a one-order of magnitude difference exists between quartz and glauconite, with regard to the modes of their grain size curves. However, the densities of these two minerals are close to each other: 2.40–2.95 g/cm^3 for glauconite versus 2.68 g/cm^3 for quartz. Consequently, such a difference between the modes cannot be accounted for by contrasted densities. Moreover, as shown in Table 3, the mode of the size-distribution curves of the quartz grains is the same for the beds as well as for the interbeds (mean values of 163 μm and 169 μm, respectively); the same holds for the sorting index (1.43 versus 1.46), as well as for the index of skewness of the quartz grain populations (0.97 versus 0.96). It is thus suggested that the energy level was the same in the two cases (bed versus interbeds) and it led to a good sorting *sensu lato* of the clastic particles. Therefore, the size difference between the glauconite grains of the carbonate beds and those of the interbeds must be accounted for by another factor (given below). The SEM observation shows that the outer aspect of the glauconite grains does not reveal systematic traces of abrasion (except for one sample), either in the beds or in the interbeds. All these results and observations imply that the two minerals where accumulated by different mechanisms. It is interpreted that the quartz has been reworked from older deposits and well sorted during remobilization, whereas the ill-sorted glauconite resulted from syn-depositional formation. It is reported above that the glauconite grains released particles of minute size during the grains size analysis. This artefact has the advantage of showing that the grains analyzed are relatively fragile. Previous works [Tribovillard et al., 2021, 2023] showed that reworked glauconite grains did not show this wear during analysis, suggesting that their more fragile cortex had been abraded during previous sedimentary stages: transport, reworking, re-deposition. This is an additional argument in favor of a syn-deposit origin of the glauconitic grains studied here. These results allowing us to conclude to syndepositional glauconite therefore support the previous interpretations of Deconinck and Baudin [2008] and Townson and Wimbledon [1979] who used the presence of glauconite as an argument in favor of the marked sedimentary condensation of the Assises of Croï.

5.1.2. *Marly interbeds*

Compared to those of the carbonate beds, the grain size patterns of the interbeds are somewhat different (Supplementary Figure S2). The curves of the grain size distribution of quartz are quite similar for the beds and the interbeds and yield modes comprised between 100 μm and 200 μm. However the

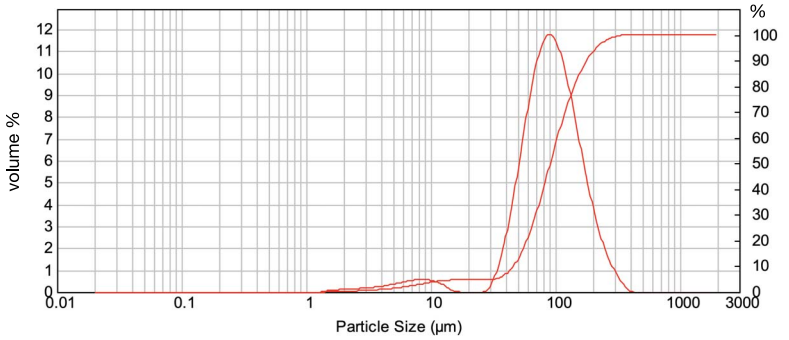

Figure 9. Typical size distribution of reworked glauconite grains (Aptian–Albian sandstones close to the Cap Blanc Nez). The sort of bump visible between 3 and 15 µm is larger than what is evoked about non-reworked glauconite.

modes of the glauconite-grain curves of the interbeds are comprised between 30 µm and 100 µm, that is, higher values compared to the carbonate beds (Supplementary Figure S2A, B). In addition, the sorting of the glauconite grains is poorer than that of the quartz grains. The similarity of the quartz modes in the beds and interbeds indicates that the energy level was the same for the two facies. Therefore, the size and sorting differences observed for glauconite when beds are compared to interbeds cannot be accounted for by contrasted conditions of depositions and must be ascribed to the diagenesis sequence itself.

5.2. *Carbonate beds of diagenetic origin*

Some observations allow a diagenetic origin of the carbonate beds to be inferred: the limestone beds have a nodular and irregular facies, they show early cemented bioturbation (Supplementary Figure S3) and are sometimes perforated by organisms. Deconinck and Baudin [2008] reached the same conclusions, based on similar observations. These few observations suggest that the carbonate beds/nodules were already firm (but not indurated) when burrowing organisms were still dwelling the sediment. The same conclusion was reached regarding the limestone–marl alternations of the Calcaires du Moulin Wibert Fm. of Kimmeridgian age, cropping out in the same area of the Boulonnais; this formation shows carbonate beds facies similar to that of the Assises de Croï [Hatem et al., 2016].

In the present case, our interpretation is further supported by stable isotope examination. The carbonate beds yield δ^{13}C values being slightly but significantly lower that those expected for Late Jurassic seawater carbonate, ranging from 0 to 2‰ V-PDB according to Veizer et al. [1999] and Prokoph et al. [2008]. The same range of ^{13}C-depleted carbonates has already been reported for the carbonate beds of the Calcaires du Moulin Wibert Fm. mentioned above as well as for the carbonate beds of the Bancs Jumeaux Fm. the least depleted in ^{13}C, both formations cropping out also along the Boulonnais coastline [Hatem et al., 2016; the Banc Jumeaux Fm. is of Tithonian age]. The carbonate beds of these two formations have been reported to be of diagenetic origin, as well as many other carbonate beds or patch reef matrices of the upper Jurassic of the Boulonnais [Tribovillard et al., 2012, Hatem et al., 2014, 2016]. In other words, the limestone beds of the Assises de Croï Fm. incorporated a fraction of biogenic ^{13}C-depleted carbon during carbonate precipitation. The values observed in the present work are slightly depleted relative to marine carbonate of late Jurassic age (see above), which suggests that the carbonate beds resulted from two mixing sources: a seawater dissolved inorganic carbon (DIC) source and an isotopically light, dissolved DIC source, most probably originating from the remineralization of organic products such as hydrocarbons and/or sedimentary organic matter [see discussion in Hatem et al., 2016].

Simultaneously, assuming a value close to (slightly above) δ^{18}O = −1‰ V-PDB for late Jurassic seawater [Veizer et al., 1999, Prokoph et al., 2008], the samples studied here are slightly depleted in ^{18}O, that is, their isotope signature is close to that of seawater. Thus, it is inferred that the carbonate beds of the Assises de Croï Fm. were influenced by diagenesis

(remineralization of organic products enriched in light carbon) during deposition (seawater-impacted isotopic signature of both C and O). Therefore, the carbonate bed formation took place during what can be termed syn-sedimentary diagenesis, as a result of rises in alkalinity probably triggered by the activity of sulfate-reducing bacteria [discussion in Hatem et al., 2016].

To conclude, the carbonate beds formed during earliest diagenesis, as shown by several visual and isotopic lines of evidences. Nevertheless, the beds contain glauconite grains that have been proved to be syn-deposit (autochthonous). Then, the question arises to assess the relative chronology of the two types of diagenetic objects: limestone beds and glauconite.

5.3. *Diagenetic sequence*

The presence of glauconite inside the carbonate objects (beds or nodules) can only be explained by the fact that this mineral was already present in the sediment when the diagenetic limestones precipitated. Indeed, the formation of glauconite requires exchanges with seawater. This condition prevents (or limits) its formation after precipitation of carbonates, which would have acted as a barrier. The formation of glauconite therefore preceded that of the limestone levels. However, it was concluded that the precipitation of carbonate was early (see above). This means that the formation of glauconite was even earlier. In support to this interpretation, it was observed that the glauconite grains were smaller in the beds than in the interbeds (Section 5.1.2). This discrepancy can be accounted for by an authigenic growth being more protracted in the interbeds relative to the beds where the precipitation of carbonate blocked up glauconite, preventing any further increase in size.

In addition, the glauconite grains of the interbeds are better sorted than those of the beds (Table 3). The grains of the interbeds are therefore larger and better sorted, but without any incidence of the energy level of the depositional environment (the quartz grains yield similar parameter values for both the beds and interbeds; Section 5.1.2). This observation may be accounted for the protracted growth of glauconite in the case of the interbeds, as if authigenic grains would tend to an "end-member" size or maximum size over the time. In the end of the growth process, the authigenic grains would fall into a relatively narrow range of size value, which would make the sorting better. Within the beds, the authigenic growth being stopped earlier or, at least, impeded, the grains would cover a larger array of size (Supplementary Figure S2).

To sum up, our results and interpretations show that the formation of glauconite preceded that of carbonate beds and nodules. This conclusion may surprise because glauconite is classically interpreted as forming slowly. The works of Odin and Matter [1981; see also Huggett et al., 2017, Huggett, 2021] report that glauconite formation may take between one or a few ky (nascent glauconite) and a few hundreds of ky (highly evolved). Glauconitization could even last up to 5 My, according to Smith et al. [1998]. The degree of maturation of glauconite is echoed by morphological and chemical criteria. Here, with $[K_2O] > 8$ wt%, $[Fe_2O_3] > 27$ wt% (or FeO > 22%) and $[Al_2O_3] > 24$ wt% [Tribovillard et al., 2023, and this work], the glauconite may be considered to be highly mature, according to Odin and Matter [1981]. Therefore, according to the current opinion mentioned above about the duration of glauconite formation, it should have lasted several hundreds of ky, which is hardly compatible with our inference that glauconite formed early in the Assises de Croï. To account for this paradox, it could be suggested that a precursor phase of green mineral such as berthierine or Fe-beidellite, known to be able to develop rapidly [Meunier and El Albani, 2007] could have formed, being later replaced by glauconite. However, if the mineral were rapidly confined within authigenic carbonate, which prevented any easy exchanges with the interstitial milieu, berthierine (or any other rapidly forming green mineral) would not have turned into glauconite. As our observations strongly suggest that glauconite formed during earlier diagenesis, it may be inferred that the so-called highly mature glauconite could also form quite rapidly. Meunier and El Albani [2007] already commented on the fact that the allegedly protracted duration of highly mature glauconite formation is hardly compatible with usual sedimentation patterns. They proposed that the long durations proposed by Odin and Matter [1981], Odin and Dodson [1982] or Smith et al. [1998] could be long time ranges during which numerous steps of rapid glauconite-grains formation took place. Meunier and El Albani [2007] could formulate their

scenario because the glauconite grains studied by Smith et al. [1998] yielded a wide range of single-grain ages. For the present work, no datations of glauconite grains are available but our sedimentological lines of evidences strongly suggest that glauconite grains, though meeting the criteria of high maturity, formed rapidly before complete cementation of the host carbonate beds and concretions. Wilmsen and Bansal [2021] drew similar conclusions for Cenomanian glauconitic strata of the Elbtal Group of Germany. Their results allowed them concluding that the glauconite formed under high-sedimentation rate conditions and on rather short timescales (as evidenced through sequence stratigraphy considerations).

In the present study, what is stressed on is the fact that carbonate objects and glauconite formed early during the diagenetic course. This is relative chronology and it does not preclude that the sedimentation rate was slow on average. However, as stated above, even if the presence of bioturbated carbonate beds and glauconite suggests that the sedimentation must have been condensed according to conventional concepts, constantly low sedimentation rate can hardly be hypothesized for such a shallow platform where clastic inputs are evidenced by omni-present quartz grains. Episodes of condensation are preferably associated with some phosphate-encrusted horizons, as well as bored and encrusted paleo surfaces, forming hard grounds or firm grounds. As said above, Wilmsen and Bansal [2021] concluded that glauconite formation was possible under high-sedimentation rate conditions.

As illustrated by Figure 7C, the chemical compositions of the glauconite grains follow the same trend and cover the same ranges, in the beds and in the interbeds. Presumably, based on larger grain size, their growth has lasted longer in interbeds than in beds. It is inferred that, in the present case, the K_2O and FeO (or Fe_2O_3) concentrations did not depend on the duration of the growth of the glauconite grains. The growth may have lasted longer in the interbeds, but it did not lead to increased K_2O concentrations relative to beds. It therefore appears that the final chemical composition was reached quickly and did not change over time. Of course, we do not intend to minimize the use of the K_2O concentration as a marker of the growth duration, we only call the attention on the fact that it must be used with caution.

6. Conclusion

Quartz and glauconite are frequently simultaneously present in sedimentary rocks. The present study shows that it can be found, within the same sediment sample, reworked quartz and syn-deposit glauconite that formed *in situ*. Here, the sedimentological characteristics observed attest to the early character of the glauconite; it would have formed before or, at the latest, during the precipitation of carbonate nodules and beds which themselves formed relatively early in the diagenetic course of these deposits. However, the glauconite examined here can be qualified as highly evolved, based on geochemical and crystallographic evidences. It can be concluded that glauconite showing signs of mineralogical maturity can nevertheless form during the early stages of diagenesis.

Acknowledgements

We thank Monique Gentric and Marion Delattre (LOG laboratory) for the financial/administrative management and the technical support of this project, respectively, and the Department of Earth Sciences of the University of Lille for its support. Thanks to Ivan Jovovic (Biogéosciences Lab, University of Dijon) for the isotope composition determination. Thanks to our referees for their useful review, thanks to Abderrazak El Albani for his constant support.

Conflicts of interest

Authors have no conflict of interest to declare.

Supplementary data

Supporting information for this article is available on the journal's website under https://doi.org/10.5802/crgeos.208 or from the author.

References

Amorosi, A. (1995). Glaucony and sequence stratigraphy: a conceptual framework of distribution in siliciclastic sequences. *J. Sedim. Res.*, B65, 419–425.

Banerjee, S., Bansal, U., Pande, K., and Meena, S. S. (2016a). Compositional variability of glauconites within the Upper Cretaceous Karai Shale Formation, Cauvery Basin, India: Implications for evaluation of stratigraphic condensation. *Sedim. Geol.*, 331, 12–29.

Banerjee, S., Bansal, U., and Thorat, U. V. (2016b). A review on palaeogeographic implications and temporal variation in glaucony composition. *J. Palaeogeogr.*, 5, 43–71.

Banerjee, S., Chattoraj, S. L., Saraswati, P. K., Dasgupta, S., and Sarkar, U. (2012). Substrate control on formation and maturation of glauconites in the Middle Eocene Harudi Formation, western Kutch, India. *Mar. Pet. Geol.*, 30, 144–160.

Bansal, U., Sundar Raju, P. V., and Banerjee, S. (2022). Compositional evolution of glauconite within Proterozoic Gandikonta Formation, Cuddapah Basin, India and its implication. In *21st International Sedimentological Congress, Beijing*. T10-90412.

Baudin, F. (2023). *La méthode Rock-Eval® : principes et applications*. ISTE-Wiley, London. (in press).

Bayliss, P. and Syvitski, J. P. M. (1982). Clay diagenesis in recent marine fecal pellets. *Geo-Mar. Lett.*, 2, 83–88.

Behar, F., Beaumont, V., and Penteado, H. L. D. B. (2001). Rock-Eval 6 technology: performances and developments. *Oil Gas Sci. Technol.*, 56, 111–134.

Bonte, A. (1969). — Le Boulonnais. *Ann. Soc. Géol. Nord*, 89, 23–46.

Bout-Roumazeilles, V., Cortijo, E., Labeyrie, L., and Debrabant, P. (1999). Clay-mineral evidence of nepheloid layer contribution to the Heinrich layers in the Northwest Atlantic. *Palaeogeogr. Palaeoclimatol. Palaeoecol.*, 146, 211–228.

Boyer, P. S., Guinness, E. A., Lynch-Blosse, M. A., and Stolzman, R. A. (1977). Greensand fecal pellets from New Jersey. *J. Sedim. Res.*, 4, 267–280.

Cohen-Sadon, H., Amrani, A., Feinstein, S., and Rosenberg, Y. O. (2022). A new empirical approach for rapid quantification of organic and pyritic sulfur in sedimentary rocks using the Rock-Eval 7S. *Org. Geochem.*, 166, article no. 104350.

Deconinck, J. F. and Baudin, F. (2008). Kimmeridgian and Tithonian sedimentary deposits of the North-Western part of the Paris Basin (Normandy and Boulonnais). *Ann. Soc. Géol. Nord*, 15(2ème série), 77–90.

Deconinck, J.-F., Chamley, H., Debrabant, P., and Colbeaux, J.-P. (1982). Le Boulonnais au Jurassique supérieur : données de la minéralogie des argiles et de la géochimie. *Ann. Soc. Géol. Nord*, 102, 145–152.

Deconinck, J. F., Geyssant, J. R., Proust, J. N., and Vidier, J. P. (1996). Sédimentologie et biostratigraphie des dépôts kimméridgiens du Boulonnais. *Ann. Soc. Géol. Nord*, 3(2ème série), 157–170.

El Albani, A., Meunier, A., and Fursich, F. (2005). Unusual occurrence of glauconite in a shallow lagoonal environment (Lower Cretaceous, northern Aquitaine Basin, SW France). *Terra Nova*, 17, 537–544.

Espitalié, J., Deroo, G., and Marquis, F. (1986). La pyrolyse Rock-Eval et ses applications — Troisième partie. *Oil Gas Sci. Technol. Rev. IFP*, 41, 73–89.

Geyssant, J. R., Vidier, J. P., Herbin, J. P., Proust, J. N., and Deconinck, J. F. (1993). Biostratigraphie et paléoenvironnement des couches de passage Kimméridgien/Tithonien du Boulonnais (Pas de Calais): nouvelles données paléontologiques (ammonites) organisation séquentielle et contenu en matière organique. *Géol. de la France*, 4, 11–24.

Hatem, E., Tribovillard, N., Averbuch, O., Sansjofre, P., Adatte, T., Guillot, F., Ader, M., and Vidier, D. (2016). Early diagenetic formation of carbonates in a clastic-dominated ramp environment impacted by synsedimentary faulting-induced fluid seepage – evidence from the Late Jurassic Boulonnais Basin (N France). *Mar. Pet. Geol.*, 72C, 12–29.

Hatem, E., Tribovillard, N., Averbuch, O., Vidier, D., Sansjofre, P., Birgel, D., and Guillot, F. (2014). Oyster patch reefs as indicators of fossil hydrocarbon seeps induced by syn-sedimentary faults. *Mar. Pet. Geol.*, 55, 176–185.

Herbin, J. P., Geyssant, J. R., El Albani, A., Colbeaux, J. P., Deconinck, J. F., Fernandez-Martinez, J. L., Proust, J. N., and Vidier, J. P. (1995). Sequence stratigraphy of source rocks applied to the study of the Kimmeridgian/Tithonian in the Northwest European shelf (Dorset/UK, Yorkshire/UK and Boulonnais/France). *Mar. Pet. Geol.*, 12, 177–194.

Huggett, J., Adetunji, J., Longstaffe, F., and Wray, D. (2017). Mineralogical and geochemical characterisation of warm-water, shallow-marine glaucony from the Tertiary of the London Basin. *Clay Miner.*, 52, 25–50.

Huggett, J. M. (2021). Glauconites. In *Encyclopedia of Geology*, pages 334–340. Elsevier, Amsterdam, 2nd edition.

Lamoureux-Var, V., Espitalié, J., Pillot, D., Bouton, N., Garcia, B., Antonas, R., Aboussou, A., Wattripont, A., Ravelojaona, H., Noirez, S., and Beau-

mont, V. (2019). Rock-Eval 7S: Technology and performance. In *29th International Meeting on Organic Geochemistry (IMOG), 1–6 September 2019, Gothenburg, Sweden*.

López-Quirós, A., Sánchez-Navas, A., Nieto, F., and Escutia, C. (2020). New insights into the nature of glauconite. *Am. Mineral.*, 105, 674–686.

Mansy, J.-L., Guennoc, P., Robaszynski, F., Amédro, F., Auffret, J.-P., Vidier, J.-P., Lamarche, J., Lefèvre, D., Sommé, J., Brice, D., Mistiaen, B., Prud'homme, A., Rohart, J.-C., and Vachard, D. (2007). *Notice explicative, carte géologique de la France (1/50 000), feuille Marquise*. BRGM, Orléans, 2nd edition.

Meunier, A. and El Albani, A. (2007). The glauconite–Fe-illite–Fe-smectite problem: a critical review. *Terra Nova*, 19, 95–104.

Odin, G. S. and Dodson, M. H. (1982). Zero isotopic age of glauconies. In *Numerical Dating in Stratigraphy*, pages 277–306. Wiley, Chichester.

Odin, G. S. and Matter, A. (1981). De glauconiarum origine. *Sedimentology*, 28, 611–641.

Prokoph, A., Shields, G. A., and Veizer, J. (2008). Compilation and time-series analysis of a marine carbonate δ^{18}O, δ^{13}C, ^{87}Sr/^{86}Sr and δ^{34}S database through Earth history. *Earth-Sci. Rev.*, 87, 113–133.

Roy Choudhury, T., Banerjee, S., Khanolkar, S., Saraswati, P. K., and Meena, S. S. (2021). Glauconite authigenesis during the onset of the Paleocene-Eocene Thermal Maximum: a case study from the Khuiala Formation in Jaisalmer Basin, India. *Palaeogeogr. Palaeoclimatol. Palaeoecol.*, 571, article no. 110388.

Smith, P. E., Evensen, N. M., York, D., and Odin, G. S. (1998). Single-grain ^{40}Ar–^{39}Ar ages of glauconies: implications for the geologic time scale and global sea level variations. *Science*, 279, 1517–1519. http://www.jstor.org/stable/2893786.

Townson, W. G. and Wimbledon, W. A. (1979). The Portlandian strata of the Bas-Boulonnais, France. *Proc. Geol. Assoc. London*, 90(1–2), 81–91.

Trentesaux, A., Récourt, P., Bout-Roumazeilles, V., and Tribovillard, N. (2001). Carbonate grain-size distribution in hemipelagic sediments from a laser particle sizer. *J. Sedim. Res.*, 71, 858–862.

Tribovillard, N., Bout-Roumazeilles, V., Abraham, R., Ventalon, S., Delattre, M., and Baudin, F. (2023). The contrasting origins of glauconite in the shallow marine environment highlight this mineral as a marker of paleoenvironmental conditions. *C. R. Geosci.*, 355(S2), 1–16.

Tribovillard, N., Bout-Roumazeilles, V., Delattre, M., Ventalon, S., Abraham, R., and Nzié, O. (2021). Syndepositional glauconite as a paleoenvironmental proxy - the lower Cenomanian Chalk of Cap Blanc Nez (N-France). *Chem. Geol.*, 584, article no. 120508.

Tribovillard, N., Sansjofre, P., Ader, M., Trentesaux, A., Averbuch, O., and Barbecot, F. (2012). Early diagenetic carbonate bed formation at the sediment–water interface triggered by synsedimentary faults. *Chem. Geol.*, 300/301, 1–13.

Veizer, J., Ala, D., Azmy, K., Bruckschen, P., Buhl, D., Bruhn, F., Carden, G. A. F., Diener, A., Ebneth, S., Godderis, Y., Jasper, T., Korte, C., Pawellek, F., Podlaha, O. G., and Strauss, H. (1999). ^{87}Sr/^{86}Sr, δ^{13}C and δ^{18}O evolution of phanerozoic seawater. *Chem. Geol.*, 161, 59–88.

Velde, B. (2014). Sediments, diagenesis and sedimentary rocks. In *Treatise on Geochemistry*, volume 9, pages 351–364. Elsevier, Amsterdam, 2nd edition.

Wilmsen, M. and Bansal, U. (2021). Depositional setting and limiting factors of early Late Cretaceous glaucony formation: implications from Cenomanian glauconitic strata (Elbtal Group, Germany). *Facies*, 67, article no. 24.